The Impact of Patches on Blood Flow Disorders In Carotid Artery

M. Ciałkowski, N. Lewandowska, M. Micker, M. Warot, A. Frąckowiak and P. Chęciński

Abstract The atherosclerotic plaques are surgically removed by endarterectomy of the common and internal carotid artery wall, removal of lesions, and suturing the artery again. To avoid arterial lumen stenosis, sewing a patch in the incision area is indicated, which will cause a slight expansion of the flow lumen. The channel expansion causes a positive tension gradient, enhancing separation of the parietal layer and occurrence of whirlpools. The latter may cause plaque redeposition. The selection of the patch size is not described in detail in the literature and is based on the surgeon's experience and intuition. The purpose of the studies is to determine the maximum patch width per surgical incision at which no flow separation will occur. To determine the geometry of the channel with a patch sewn in, an equation was determined to reflect the course of the arterial wall curves by math functions. The artery radius, the maximum expansion radius, and the length of the patch sewn in have been assumed as the input parameters that define the boundary conditions necessary for the determination of polynomial coefficients. By a gradual increase of the maximum radius, a geometry group was determined, which was the starting point for numerical simulations. The simulations were made with the use of Fluent. The increasing of the maximum radius was continued until the separation of the parietal layer was detected and whirlpools occurred. The results showed that when the maximum radius is 30% greater in relation to the arterial radius, whirlpools occur, which in consequence may lead to plaque redeposition.

M. Ciałkowski · N. Lewandowska (✉)
Faculty of Machines and Transport, Poznan University of Technology, Chair of Thermal Engineering, Piotrowo 3, 60-695 Poznan, Poland
e-mail: natalia.lewandowska.pp@gmail.com

M. Micker · M. Warot · A. Frąckowiak · P. Chęciński
Department of General and Vascular Surgery and Angiology, Poznan University of Medical Sciences (PUMS), 34 Dojazd St, 60-631 Poznan, Poland

J. M. R. S. Tavares and P. R. Fernandes (eds.), *New Developments on Computational Methods and Imaging in Biomechanics and Biomedical Engineering*, Lecture Notes in Computational Vision and Biomechanics 33, https://doi.org/10.1007/978-3-030-23073-9_1

1 Introduction

Atherosclerotic plaques very often deposit at the points of carotid artery bifurcation, which might result in a closure of the arterial lumen. According to the experimental research [1, 2, 3], when the stenosis level in the arterial lumen reaches ca. 60–75%, it is necessary to remove the arterial lesions surgically. This operation is a generally accepted form of primary or secondary ischemic stroke prophylactics [4]. The plaques are most frequently removed by means of lengthwise incision of the artery wall, removal of the adhering plaque and resuturing of the artery. It is also possible to cut off the internal carotid artery, extract of the atherosclerotic plaque and reconnect the cutoff artery. This procedure, however, is less frequent. Direct suturing of the membrane (Fig. 1a) causes artery lumen stenosis. This is a negative phenomenon as it reduces the arterial flow capacity and may cause disorders. Both factors mentioned above cause an increased restenosis probability. Considering the said prerequisites, experienced surgeons recommend insertion at the point of the artery incision of a patch (Fig. 1b) made of plastic (usually dacron or polytetrafluoroethylene—PTFE) or tissue taken from the patient (most frequently a vein). Dacron, however, is the most commonly used material. The application of a patch reduces the risk of a stroke, death, or restenosis as compared to the primary suturing of the wound after the arteriotomy [5, 6]. It eliminates the risk of arterial lumen stenosis, but in turn, causes its expansion. The patch width is selected directly on the operating table when the surgeon adjusts the appropriate patch geometry based on his/her own experience. There is no scientific justification of the selected patch geometry—its width is fixed intuitively in most cases. This paper presents an attempt of an analytic and mathematical determination of the geometry of the patches that minimize the risk of restenosis.

From the mechanical point of view, the flow through the divergent canal enhances the separation of the layer adhering to the wall and a formation of a reverse flow near the walls. The occurring whirlpools may cause ‘suction’ of solid particles into

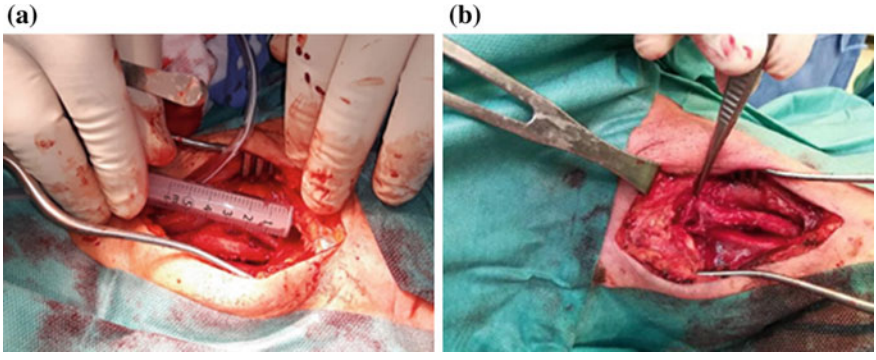

Fig. 1 Plague removal surgery: **a** with a patch **b** without a patch

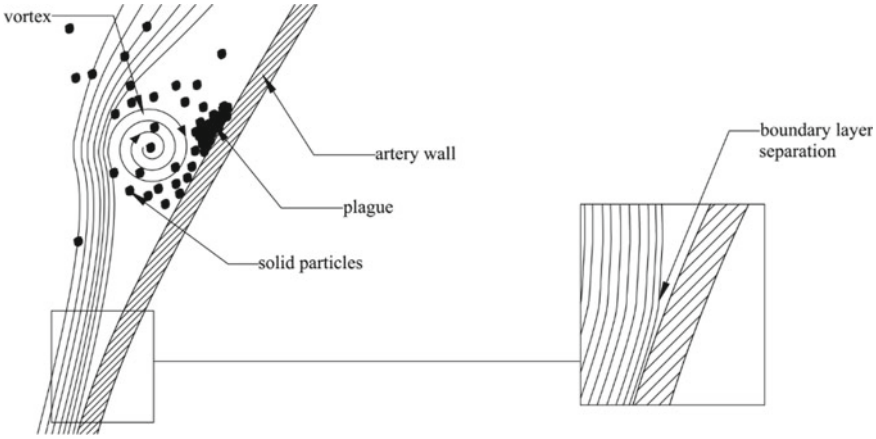

Fig. 2 Schematics of the basic concept of boundary layer separation

the center, which in consequence, may lead to plaque redeposition near the wall. Figure 2 presents the concept of this phenomenon.

Upon respective expansion of the arterial canal, whirlpools occur in the blood flow, which in consequence may lead to plaque redeposition on the walls.

The purpose of the studies is to determine the geometry of a patch that would not cause flow turbulization when inserted in the carotid artery. The research works considered analytical and numerical computation. The developed geometric models were based on the analytical results and represented a basis for the numerical computation. A series of simulations was carried out to show the impact of the geometry on the parameters characterizing the flow. The analysis results showed that whirlpools begin to appear near the walls when the artery diameter is expanded by more than 30%, compared to its original dimension. This corresponds to the maximum patch width of 10–14 mm, depending on the arterial diameter. The geometry of the patch that would not lead to restenosis has been developed based on the obtained results. The research results represent the first fully documented analysis concerning the geometry of the inserted patches. They may constitute the foundations for the selection of a specific patch width, customized to the geometry of a patient's artery.

2 Methods

2.1 Mathematical Analysis

The patch geometry was determined by means of three functions: fourth-degree polynomial, a spline function composed of two cubic polynomials and the ellipsis

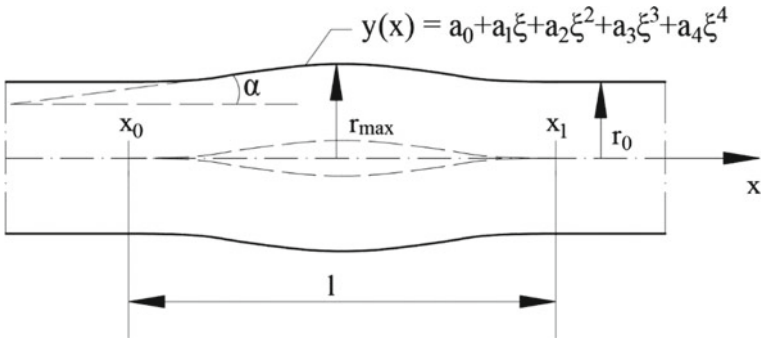

Fig. 3 Patch geometry

function. The numerical tests showed that the ellipsis is the least favorable function. Both polynomial functions under analysis yielded similar results.

2.1.1 Fourth-Degree Polynomial

The following fourth-degree polynomial was used to describe the expanded artery (Fig. 3):

$$y(x) = a_0 + a_1 \frac{x - x_0}{x_1 - x_0} + a_2 \left(\frac{x - x_0}{x_1 - x_0} \right)^2 + a_3 \left(\frac{x - x_0}{x_1 - x_0} \right)^3 + a_4 \left(\frac{x - x_0}{x_1 - x_0} \right)^4 \quad (1)$$

Introduction of a dimensionless variable $\xi = (x - x_0)/(x_1 - x_0)$ results in the following function:

$$y(\xi) = a_0 + a_1 \xi + a_2 \xi^2 + a_3 \xi^3 + a_4 \xi^4 \quad (2)$$

To determine the polynomial coefficients, the following boundary conditions have been applied:

- smooth connection of the part of unvaried diameter with the expanded part:

$$y(\xi = 0) = y(\xi = 1) = r_0 \quad (3)$$

- equality of tangents:

$$y'(\xi = 0) = y'(\xi = 1) = 0 \quad (4)$$

- maximum artery expansion radius:

$$y\left(\xi = \frac{1}{2}\right) = r_{max} \tag{5}$$

After implementing above boundary conditions, polynomial coefficients values are equal:

$$\begin{cases} a_0 = r_0 \\ a_1 = 0 \\ a_2 = 16(r_{max} - r_0) \\ a_3 = -32(r_{max} - r_0) \\ a_4 = 16(r_{max} - r_0) \end{cases} \tag{6}$$

Upon determination of the polynomial coefficients, function assumes the following form:

$$y(\xi) = r_0 + 16 \cdot (r_{max} - r_0) \cdot \xi^2 \cdot (1 - \xi)^2, \xi = \frac{x - x_0}{x_1 - x_0} = \frac{x - x_0}{l}, x = x_0 + l \cdot \xi \tag{7}$$

The angle of inclination of the variable edge to the x-axis is

$$tg\alpha(\xi) = \frac{dy}{dx} = \frac{dy}{d\xi} \cdot \frac{d\xi}{dx} = \frac{dy}{ld\xi} = \frac{1}{l} \cdot 32(r_{max} - r_0)\xi(1 - \xi) \cdot (1 - 2\xi) \tag{8}$$

while the extreme inclination angle results from zeroing of I derivative, namely

$$(tg\alpha(\xi))' = 32(r_{max} - r_0)\left(1 - 6\xi + 6\xi^2\right)/l = 0 \tag{9}$$

which occurs for

$$\xi_1^* = \frac{1}{2} - \frac{1}{2} \cdot \frac{1}{\sqrt{3}} = \frac{1}{2}\left(1 - \frac{1}{\sqrt{3}}\right) \approx 0.211 \tag{10}$$

$$\xi_2^* = \frac{1}{2}\left(1 + \frac{1}{\sqrt{3}}\right) \approx 0.789 \tag{11}$$

whereas

$$\left(tg\alpha\left(\xi_1^*\right)\right)'' = -192(r_{max} - r_0) \cdot \left(1 - 2\xi_1^*\right)/l < 0 \tag{12}$$

therefore angle $\alpha\left(\xi_1^*\right)$ reaches its maximum value.

For $\xi = \xi_2^*$, the tangent function drops to its minimum value, because angle α is an obtuse angle.

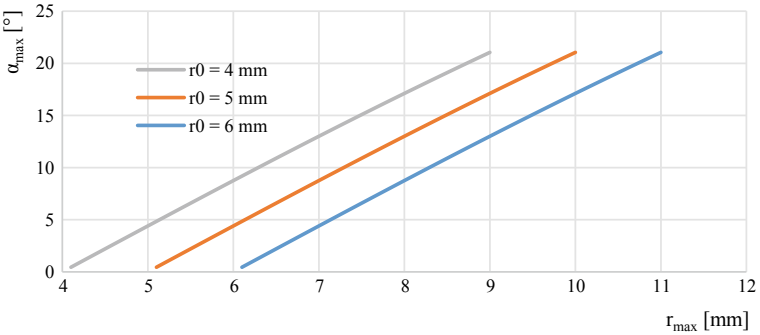

Fig. 4 Function of the maximum angle of inclination for different value of artery radius (r_0) and the constant value of patch width $l = 40$ mm

Parameter r/r_{max} is related to angle $\alpha_{max} = \alpha\left(\xi = \xi_1^*\right) = \alpha\left(\xi = \frac{1}{2}\left(1 - \frac{1}{\sqrt{3}}\right)\right)$

$$tg\alpha_{max} = 32\frac{r_{max} - r_0}{l} \cdot \xi(1-\xi)(1-2\xi) \tag{13}$$

$$tg\alpha_{max} = 32\frac{r_{max} - r_0}{l}\frac{1}{2}\left(1 - \frac{1}{\sqrt{3}}\right)\frac{1}{2}\left(1 + \frac{1}{\sqrt{3}}\right)\frac{1}{\sqrt{3}} = \frac{16}{3\sqrt{3}} \cdot \frac{r_{max} - r_0}{l} \tag{14}$$

$$\alpha_{max} = \text{arc}\,tg\frac{16}{3\sqrt{3}} \cdot \frac{r_{max} - r_0}{l} = \text{arc}\,tg\frac{16}{3\sqrt{3}} \cdot \frac{r_0}{l}\left(\frac{r_{max}}{r_0} - 1\right) \tag{15}$$

or

$$r_{max} = r_0 + \frac{3\sqrt{3}}{16} \cdot l \cdot tg\alpha_{max} \tag{16}$$

Angle α_{max} for the outline described by function (Eq. 15) will result from a flow without separation, being the Reynolds number function. As initial value for further calculation there will be assumed $\alpha_{max} = 10°$ then

$$r_{max} = r_0 + 3\sqrt{3} \cdot 16^{-1} \cdot 0.003046 \cdot l = r_0 + 0.00099 \cdot l \tag{17}$$

for $\alpha_{max} = 45°$ $l = 40$ mm, $r_0 = 5$ mm

$$r_{max} = r_0 + \frac{3\sqrt{3}}{16} \cdot 1 \cdot l = r_0 + 0.3248\,l$$

$$r_{max} = 5 + 13 = 18 \text{ mm},\ r_{max}/r_0 = 1 + 2.6 = 3.6,$$

which is an unreal result. In Figs. 4, 5, 6, 7 charts $\alpha_{max} = f(r_{max})$ and $r_{max} = f(r_0, \alpha_{max})$ are presented.

Patch width

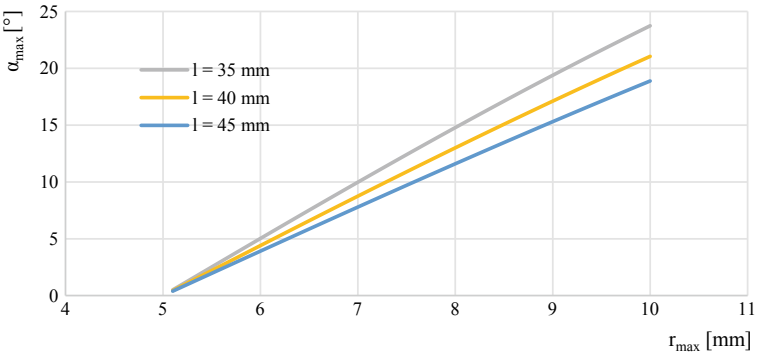

Fig. 5 Function of the maximum angle of inclination for different value of patch length (l) and the unchanged value of artery diameter ($r_0 = 5$ mm)

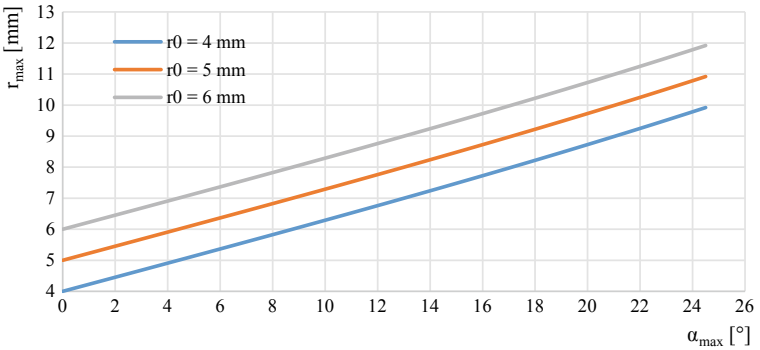

Fig. 6 Function of the maximum radius in the widening part of artery for different values of artery radius (r_0) and the patch length $l = 40$ mm

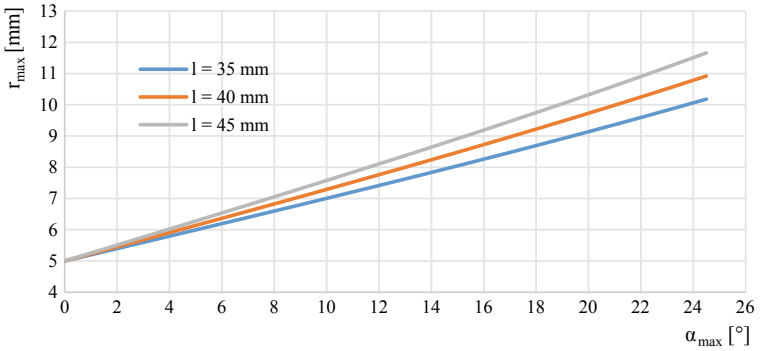

Fig. 7 Function of the maximum radius in the widening part of artery for different values of patch length (l) and the artery radius $r_0 = 5$ mm

The perimeter patch width is the result of the relation

$$s(\xi) = 2\pi \cdot y(\xi) - 2\pi r_0 = 32\pi(r_{max} - r_0)\xi^2(1-\xi)^2 \tag{18}$$

and reaches its maximum in the center $\xi = 0.5$

$$s_{max} = 2\pi(r_{max} - r_0) \tag{19}$$

or

$$\frac{s_{max}}{2\pi r_0} = \frac{r_{max}}{r_0} - 1 \tag{20}$$

The parameter $\zeta = r_{max}/r_0$ was introduced to the numerical computation, then

$$y(\xi) = r_0 \cdot \left[1 + 16\left(\frac{r_{max}}{r_0} - 1\right)\xi^2(1-\xi)^2\right] = r_0 \cdot \left[1 + 16(\zeta - 1)\xi^2(1-\xi)^2\right] \tag{21}$$

or in the dimensionless form

$$\frac{y(\xi)}{r_0} = 1 + 16(\zeta - 1)\xi^2(1-\xi)^2 \tag{22}$$

$$\alpha_{max} = \text{arc tg}\left(\frac{16}{3\sqrt{3}} \cdot \frac{r_0}{1}(\zeta - 1)\right) \tag{23}$$

$$\frac{s_{max}}{2\pi} = r_0(\zeta - 1) \rightarrow \frac{s_{max}}{2\pi r_0} = \zeta - 1 \tag{24}$$

value $s_{max}/2\pi$ expresses the artery radius increase at the widest point of the patch insertion, while $s_{max}/2\pi r_0$ is the dimensionless growth of the radius.

Assuming that $r_0 = 5$ mm, $l = 40$ mm, $\zeta \leq 1.3$ the argument of function (21) is

$$\frac{16}{3\sqrt{3}} \cdot \frac{5}{40} \cdot (1.3 - 1) = 0.11547 \Rightarrow \text{arc tg } 0.11547 = 0.1149 \text{ rd} = 6.587^\circ,$$

on the other hand

$$\text{arc tg } x = x - \frac{x^3}{3} + \frac{x^5}{5} = 0.11547 - 0.00051 = 0.11493 \text{ rd}$$

while the omission of higher exponents leads to expression

$$\text{arc tg } x = x \cdots = 0.11547 \text{ rd} = 6.616^\circ$$

which produces the relative error

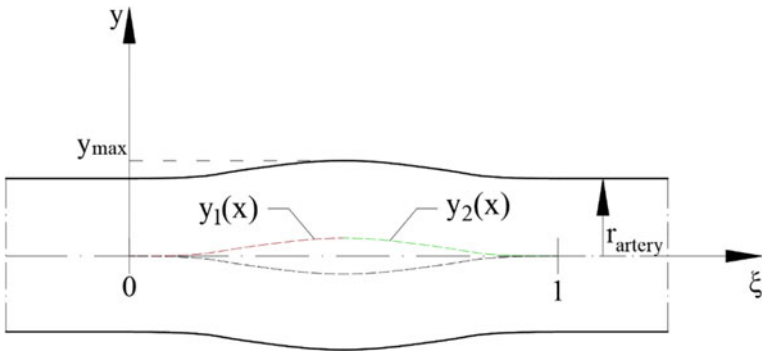

Fig. 8 Analytical description of the spline function

$$\delta = \frac{6.587^\circ - 6.616^\circ}{6.587^\circ} \cdot 100\% \approx 0.44\%$$

So, in the interval $\alpha_{\max} \leq 6,5^\circ$, we obtain a simple dependency between the maximum radius and the corresponding maximum inclination angle of the tangent to the artery outline

$$\alpha_{\max} = \frac{16}{3\sqrt{3}} \cdot \frac{1}{8}\left(\frac{r_{\max}}{5} - 1\right) \rightarrow r_{\max} = 5\left(1 + \frac{3\sqrt{3}}{2}\alpha_{\max}\right) \tag{25}$$

The patch width in the widest part of the artery (for $r_0 = 5$ mm and $\zeta = 1.3$)

$$s_{\max} = 2\pi r_0(\zeta - 1) = 2\pi \cdot 5(1,3 - 1) = 9.42 \text{ mm}$$

2.1.2 Third-Degree Polynomial Spline

Patch, in this case, is described by two third-degree polynomial functions (Fig. 8):

$$y_1(\xi) = a_0 + a_1\xi + a_2\xi^2 + a_3\xi^3 \tag{26}$$

$$y_2(\xi) = b_0 + b_1\xi + b_2\xi^2 + b_3\xi^3 \tag{27}$$

Conditions on the curve ends

$$y_1(0) = a_0 = 0 \tag{28}$$

$$y_1'(0) = a_1 = 0 \tag{29}$$

$$y_2(1) = b_0 + b_1 + b_2 + b_3 = 0 \tag{30}$$

$$y_2'(1) = b_1 + 2b_2 + 3b_3 = 0 \tag{31}$$

$$y_1\left(\xi = \frac{1}{2}\right) = y_2\left(\xi = \frac{1}{2}\right) = r_{max} \tag{32}$$

which leads to

$$y_1(\xi) = a_2\xi^2 + a_3\xi^3 \tag{33}$$

$$y_1'(\xi) = 2a_2\xi + 3a_3\xi^2 \tag{34}$$

Convergence conditions at center point $\xi = 1/2$:

$$y_1\left(\frac{1}{2}\right) = \frac{1}{4}a_2 + \frac{1}{8}a_3 = y_{max} \tag{35}$$

$$y_1\left(\frac{1}{2}\right) = y_2\left(\frac{1}{2}\right) \Rightarrow \frac{1}{4}a_2 + \frac{1}{8}a_3 = b_0 + \frac{1}{2}b_1 + \frac{1}{4}b_2 + \frac{1}{8}b_3 \tag{36}$$

$$y_1'\left(\frac{1}{2}\right) = y_2'\left(\frac{1}{2}\right) \Rightarrow a_2 + \frac{3}{4}a_3 = b_1 + b_2 + \frac{3}{4}b_3 \tag{37}$$

$$y_1''\left(\frac{1}{2}\right) = y_2''\left(\frac{1}{2}\right) \Rightarrow 2a_2 + 6a_3 \cdot \frac{1}{2} = 2b_2 + 3b_3 \tag{38}$$

We have 8 equations with 8 unknowns ($a_0 = a_1 = 0$).

$$\begin{gathered} b_0 + b_1 + b_2 + b_3 = 0 \\ b_1 + 2b_2 + 3b_3 = 0 \\ \tfrac{1}{4}a_2 + \tfrac{1}{8}a_3 = y_{max} \\ \tfrac{1}{4}a_2 + \tfrac{1}{8}a_3 = b_0 + \tfrac{1}{2}b_1 + \tfrac{1}{4}b_2 + \tfrac{1}{8}b_3 \\ a_2 + \tfrac{3}{4}a_3 = b_1 + b_2 + \tfrac{3}{4}b_3 \\ 2a_2 + 3a_3 = 2b_2 + 3b_3 \end{gathered} \tag{39}$$

$$\begin{bmatrix} \frac{1}{4} & \frac{1}{8} & 0 & 0 & 0 & 0 \\ \frac{1}{4} & \frac{1}{8} & -1 & -\frac{1}{2} & -\frac{1}{4} & -\frac{1}{8} \\ 1 & \frac{3}{4} & 0 & -1 & -1 & -\frac{3}{4} \\ 2 & 3 & 0 & 0 & -2 & -3 \\ 0 & 0 & 1 & 1 & 1 & 1 \\ 0 & 0 & 0 & 1 & 2 & 3 \end{bmatrix} \begin{Bmatrix} a_2 \\ a_3 \\ b_0 \\ b_1 \\ b_2 \\ b_3 \end{Bmatrix} = \begin{bmatrix} 1 & 0 & 0 & 0 & 0 & 0 \\ 0 & & & & & \vdots \\ 0 & & & & & \vdots \\ 0 & & & & & \vdots \\ 0 & & & & & \vdots \\ 0 & \cdots & \cdots & \cdots & \cdots & 0 \end{bmatrix} \begin{Bmatrix} y_{max} \\ 0 \\ \vdots \\ \vdots \\ \vdots \\ 0 \end{Bmatrix}$$

The solution of the system of equations is as follows:

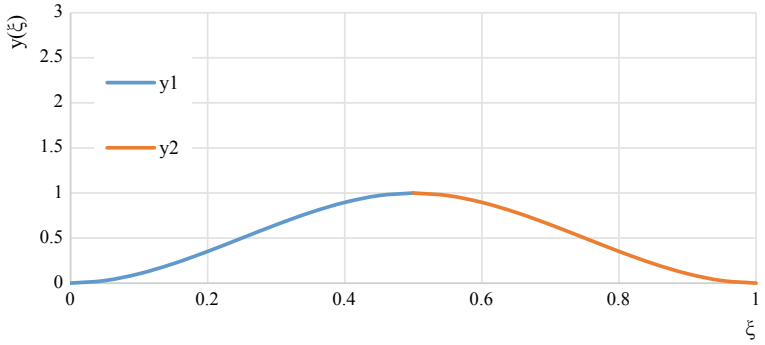

Fig. 9 Function of patch geometry composed of two third-polynomial functions described by Eqs. 41, 42

$$\begin{aligned} a_0 = a_1 = 0 \quad a_2 = 12 \cdot y_{max} \; a_3 = -16 \cdot y_{max} \\ b_0 = -4 \cdot y_{max} \; b_1 = 24 \cdot y_{max} \; b_2 = -36 \cdot y_{max} \; b_3 = 16 \cdot y_{max} \end{aligned} \tag{40}$$

Third-degree curves that fulfil the conditions of zeroing the I derivative in $\xi = 0$ and $\xi = 1$ are described by functions:

$$y_1(\xi) = 12y_{max}\xi^2 - 16y_{max}\xi^3 = 4y_{max}\xi^2(3 - 4\xi) \tag{41}$$

$$y_2(\xi) = -4y_{max} + 24y_{max}\xi - 36y_{max}\xi^2 + 16y_{max}\xi^3 \tag{42}$$

In Fig. 9, the curve composed of Eqs. 41, 42 and for $y_{max} = 1$ is presented.

The maximum curve y_1 inclination angle is at the point where the first derivative of the tangent's tangent is zeroed.

$$\frac{dy_1}{d\xi} = tg\alpha(\xi) = 0 \tag{43}$$

The inclination angle reach the maximum value 2nd derivative of function y_1 is equal to 0.

$$\frac{d}{d\xi}\left(\frac{dy_1}{d\xi}\right) = \frac{d}{d\xi}\left(\frac{d}{d\xi}\left(\frac{1}{2}\xi^2 - 16\xi^3\right)y_{max}\right) = 96y_{max}\left(\frac{1}{4} - \xi\right) = 0 \tag{44}$$

The maximum takes place at point $\xi_1^* = 0.25$, because $tg\alpha\left(\xi_1^*\right)'' < 0$.
For the function y_2:

$$\frac{d}{d\xi}\left(\frac{dy_2}{d\xi}\right) = \left(-4 + 24\xi - 26\xi^2 + 16\xi^3\right)'' \cdot y_{max} = (-72 + 96\xi) \cdot y_{max} = 0 \tag{45}$$

Therefore $\xi_2^* = 0.75$.
For interval $\xi \in \langle 0, \frac{1}{2} \rangle$ and $y_{max} = r_{max}$ based on Eq. 40

$$y(\xi) = 16 \cdot \left(\frac{3}{4} - \xi \right) \cdot \xi^2 \cdot r_{max} \tag{46}$$

while for $\xi \in \langle \frac{1}{2}, 1 \rangle$

$$y(\xi) = \left(-4 + 24\xi - 36\xi^2 + 16\xi^3 \right) \cdot r_{max} \tag{47}$$

therefore

- interval $\xi \in \langle 0, 1/2 \rangle$

$$\frac{dy}{dx} = \frac{dy}{d\xi} \cdot \frac{d\xi}{dx} = \frac{dy}{d\xi} \cdot \frac{d}{dx}\left(\frac{x - x_0}{l} \right) = \zeta \cdot \frac{1}{l} \cdot tg\alpha(\xi), \zeta = \frac{r_{max}}{r_0} \tag{48}$$

- interval $\xi \in \langle 1/2, 1 \rangle$

$$\frac{dy}{dx} = \frac{1}{l} \cdot \frac{dy}{d\xi} = \zeta \cdot \frac{r_0}{l} \cdot tg\alpha(\xi), \zeta = \frac{r_{max}}{r_0} \tag{49}$$

The patch width

- interval $\xi \in \langle 0, \frac{1}{2} \rangle$

$$\begin{aligned} s(\xi) &= 2\pi y(\xi) - 2\pi r_0 = 2\pi(y(\xi) - r_0) = 2\pi \left[16\xi^2 \left(\frac{3}{4} - \xi \right) r_{max} - r_0 \right] \\ &= 2\pi r_0 \cdot \left[16\xi^2 \left(\frac{3}{4} - \xi \right) \frac{r_{max}}{r_0} - 1 \right] = 2\pi r_0 \left[16\xi^2 \left(\frac{3}{4} - \xi \right) \cdot \zeta - 1 \right], \zeta = \frac{r_{max}}{r_0} \end{aligned} \tag{50}$$

- interval $\xi \in \langle \frac{1}{2}, 1 \rangle$

$$\begin{aligned} s(\xi) &= 2\pi y(\xi) - 2\pi r_0 = 2\pi \cdot 4\left(-1 + 6\xi - 9\xi^2 + 4\xi^3 \right) \cdot r_{max} - 2\pi r_0 \\ &= 2\pi r_0 \left[4\left(-1 + 6\xi - 9\xi^2 + 4\xi^3 \right) \frac{r_{max}}{r_0} - 1 \right] \\ &= 2\pi r_0 \left[4\left(-1 + 6\xi - 9\xi^2 + 4\xi^3 \right) \zeta - 1 \right] \end{aligned} \tag{51}$$

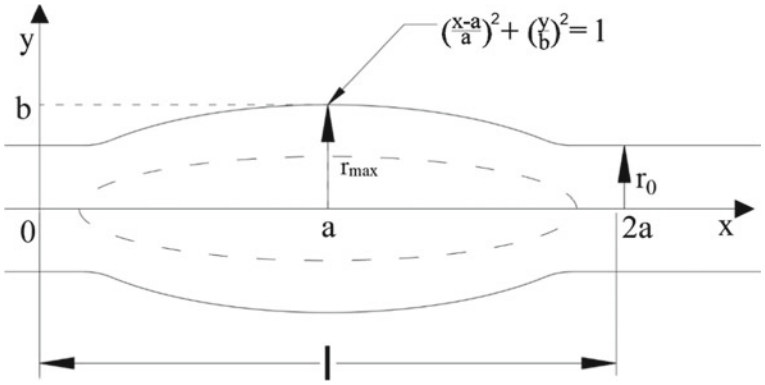

Fig. 10 Elliptical patch

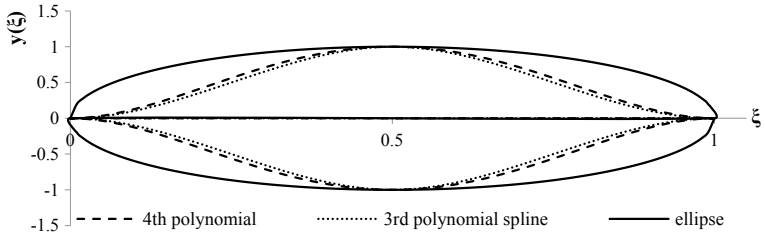

Fig. 11 Comparison of patch geometries

2.1.3 Elliptical Patch

The elliptical equation takes the following form Figs. 10, 11:

$$\left(\frac{x-a}{a}\right)^2+\left(\frac{y}{b}\right)^2=1 \tag{52}$$

Upon introduction of a dimensionless coordinate $\xi=\frac{x}{l}\rightarrow x=\xi\cdot l$ Eq. (1) takes the form

$$\left(\frac{\xi\cdot l-a}{a}\right)^2+\left(\frac{y}{b}\right)^2=1 \tag{53}$$

therefore

$$y=\pm b\sqrt{1-\left(\frac{l}{a}\xi-1\right)^2} \tag{54}$$

The perimeter of artery (with radius r_0) with inserted elliptical path is ($l=2a$)

$$p(\xi) = 2\pi r_0 + 2y = 2\pi r_0 + 2b\sqrt{1 - (2\xi - 1)^2} \tag{55}$$

therefore, the variable artery radius

$$r(\xi) = \frac{p(\xi)}{2\pi} = r_0 + \frac{b}{\pi}\sqrt{1 - (2\xi - 1)^2} \tag{56}$$

and for $\xi = 1/2$

$$r_{max} = r\left(\frac{1}{2}\right) = r_0 + \frac{b}{\pi} \tag{55}$$

For the model case $r_0 = 5$ mm, b = 4 m, $l = 40$ mm

$$r_{max} = 5 + \frac{4}{\pi} \approx 6,27 \approx 6,3\,\text{mm} \tag{56}$$

whereas $b = r_{max} - r_0$, therefore

$$y(\xi) = r_0 + (r_{max} - r_0)\sqrt{1 - (2\xi - 1)^2},\ \xi = \frac{x}{l} \rightarrow d\xi = \frac{1}{l}dx \tag{57}$$

$$\frac{dy}{dx} = \frac{dy}{d\xi} \cdot \frac{d\xi}{dx} = \frac{1}{l}\frac{dy}{d\xi} = \frac{r_{max} - r_0}{l} \cdot \frac{d}{d\xi}\sqrt{1(2\xi - 1)^2}$$
$$= \frac{r_0}{l}\left(\frac{r_{max}}{r_0} - 1\right) \cdot \frac{-2(2\xi - 1)}{\sqrt{1 - (2\xi - 1)^2}} = tg\alpha(\xi),\ \xi \in \langle 0, 1\rangle \tag{58}$$

It is conspicuous that for $\xi = 1$ $\alpha = 90°$. The angle of the tangent to curve $y(\xi)$ decreases from 90° to 0° in the interval $\xi \in \left\langle 0, \frac{1}{2}\right\rangle$ and further grows to 90° for $\xi = 1$.

Patch width

The perimeter width of the patch is

$$s(\xi) = 2\pi y(\xi) - 2\pi r_0 = 2\pi r_0(\zeta - 1)\sqrt{1 - (2\zeta - 1)^2}, \zeta = \frac{r_{max}}{r_0} \tag{59}$$

or in the dimensionless form

$$\frac{s(\xi)}{2\pi r_0} = (\zeta - 1) \cdot \sqrt{1 - (2\xi - 1)^2}, \xi \in \langle 0, 1\rangle \tag{60}$$

2.2 Summary

Figure 6 presents a comparison of the patch width curve determined by the function:

- polynomial:

$$y(\xi) = 16\xi^2(1-\xi)^2,\ \xi \in \langle 0, 1\rangle \tag{61}$$

- spline:

$$y(\xi) = 12\xi^2 - 16\xi^3, \xi \in \left\langle 0, \frac{1}{2}\right\rangle \tag{62}$$

$$y(\xi) = -4 + 24\xi - 36\xi^2 + 16\xi^3, \xi \in \left\langle \frac{1}{2}, 1\right\rangle \tag{63}$$

- elliptical:

$$y(\xi) = \sqrt{1-(2\xi-1)^2}, \xi \in \langle 0, 1\rangle \tag{64}$$

2.3 Numerical Analysis

To obtain a full description of fluid flow kinematics, a system of equations is solved describing the principles of conservation of momentum and mass, which form the basis to calculate velocity, pressure, density and temperature. No analytical solution of the general Navier–Stokes equation has been found, therefore the determination of an accurate solution is impossible from the analytical point of view. However, satisfactory solutions are obtainable approximating the solution of the equation by numerical methods. In the case of the research carried out herein, this was the finite volume method [7, 8, 9].

To describe a variation of any physical value in space and time, transport equations are used, also referred to as the conservation equations. To describe blood flow in the arteries, two equations are used:

- momentum transport equation:

$$\rho\left(\frac{\partial u_i}{\partial t} + u_j\frac{\partial u_i}{\partial x_i}\right) = -\frac{\partial p}{\partial x_i} + \mu\frac{\partial^2 u_i}{\partial x_j \partial x_j} \tag{65}$$

- mass transport equation:

$$\frac{\partial u_i}{\partial x_i} = 0 \tag{66}$$

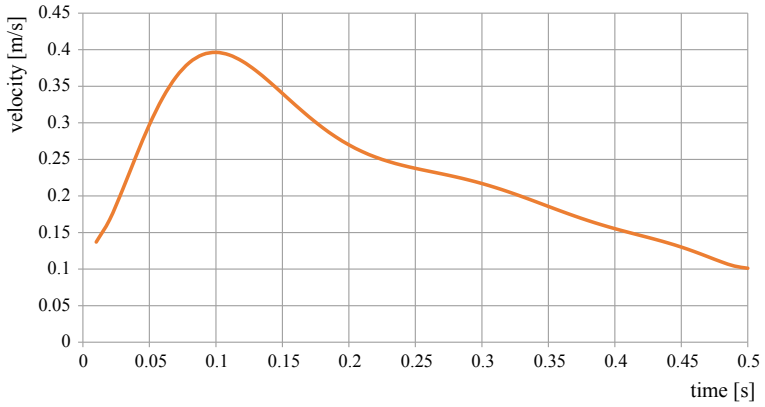

Fig. 12 Inlet velocity profile (one pulse duration = 0.5 s)

After the numerical solution of the above equations, the components of velocity and pressure are obtained, which enables the acquisition of full knowledge of the flow nature. The system of equations described above, due to the assumption of averaged velocity value (Reynolds distribution), must be supplemented with additional equations considering the velocity fluctuations. The additional system of equations is called the turbulence model. The k-ω SST model was selected for the research, due to its versatility and efficient detection of separations of the wall layer [9, 10]. An additional parameter determined by the said equations is the kinetic energy of turbulence defining the energy of whirlpools occurring in the flow. The larger and stronger the whirlpools, the higher the value of the kinetic energy of turbulence. Thanks to this property, this parameter is the foundation for the arterial flow assessment in terms of turbulence.

A nonstationary, pulsating velocity profile was applied at the artery inlet. Figure 12 presents the course of one cycle, which takes 0.5 s. The selected velocity profile was prepared based on ultrasound test results and data found in relevant literature [11, 12]. The maximum velocity is 0.4 m/s. The curve presenting velocity was shown in Fig. 12. The curve is described by the polynomial function. At the outlets, the zero-pressure boundary condition was applied [12, 13]. This is determined by the fact that the primary purpose of the study is to define the impact of the geometry on the flow. The introduction of the pulsating outlet pressure profile could have caused some additional disorders, physically unrelated to the purpose of this study. In order to examine the impact of the velocity on the flow, a series of simulations were made for the pulsating velocity profile of the maximum value of 1 m/s. Its curve is identical and the only difference is the amplitude.

Blood is a liquid of a viscosity highly dependent on the velocity of the flow. This dependency is not linear, therefore blood is classified in the non-Newtonian group of fluids. At low velocities the viscosity value is very high. It enhances the proneness of the wall layer to separate as well as the occurrence of whirlpools compared to the

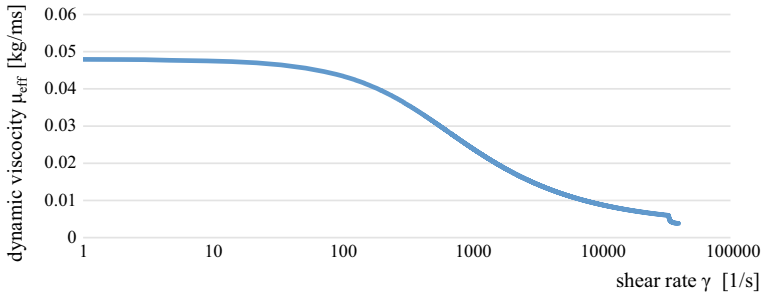

Fig. 13 Carreau function

Newtonian fluids such as water [14, 15]. In the course of the research, the Carreau model [16, 17, 18, 12]. The Carreau formula is presented by Eq. 67. In Fig. 13, change of dynamic viscosity as a function of shear rate is presented. The coefficients in Eq. 67 were selected based on the experimental tests [17].

$$\mu_{\text{eff}}(\dot{\gamma}) = \mu_{\infty} + (\mu_0 - \mu_{\infty})\left(1 + (\lambda\dot{\gamma})^2\right)^{\frac{n-1}{2}} \tag{67}$$

of which:

$\dot{\gamma}\left[s^{-1}\right]$—deformation of velocity given by the formula:

$$\dot{\gamma} = \frac{\partial u_i}{\partial x_i}\tau^{-1} \tag{68}$$

$\lambda = 3.13$ s—fluid relaxation time

$n = 0.3568$—exponent

$\mu_{\infty} = 0.00345$ kg/m·s—viscosity value at indefinitely high coagulation velocity (in the flow core),

$\mu_0 = 0.056$ kg/m·s—viscosity value at zero coagulation velocity (near the walls).

3 Results

Based on the equations obtained in the analytical parts, several geometries have been produced. The obtained models can be divided into three groups, differing by artery diameters. In each group, the artery expansions from 10% of the original dimension to 50% were examined. The examinations were made for unilateral expansion of the patch. Figure 14 presents the results of the simulation for the same expansion level, with a symmetrical expansion in the first case and unilateral in the second. It is noticeable that in the nonsymmetrical case the created whirlpool is larger, which makes the plaque deposition more probable. With the symmetrical expansion, the whirlpools are smaller, because they occur in two locations. The conclusion of such

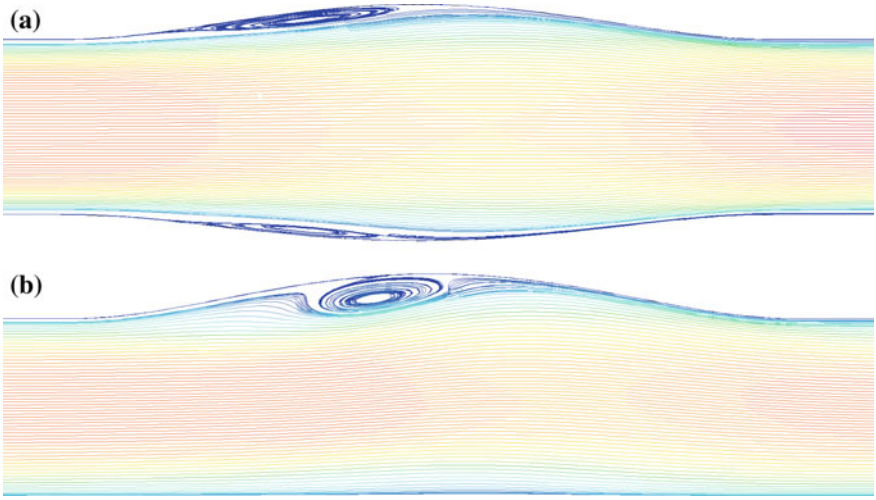

Fig. 14 Dilation of the artery: **a** symmetric **b** asymmetric

a comparison is that cases of unilateral expansion are worse in terms of the flow. They also occur more frequently in practice, particularly when the patch is inserted near the carotid artery bifurcation area, which is the major object of the study.

Figure 15 presents the curve of the current line for the patch described by grade 4 polynomial and the patch described by the function composed of grade 3 polynomials (spline). It can be observed that the curve of the current line is practically the same. Therefore, only one geometry was examined (function composed of third-grade polynomials—due to its higher accuracy).

The geometry defined by the elliptical function is the most approximate to the patches inserted presently. Figure 16a presents the current lines for the elliptical case. The graphical presentation Fig. 16b shows the results for the polynomial patch with the same maximum expansion radius. The conclusion of the drawing can be that the flow through the elliptical geometry causes whirlpools already at a 20% expansion, while no whirlpools occur in the elliptical patch. This is the main reason for the application of polynomial patches.

Based on the above preliminary studies, the authors chose to carry out a detailed examination of unilateral expansions occurring upon the insertion of the patch defined by a polynomial function. For each group of geometries, the value of the coefficient of stenosis was determined defined by the ratio of the maximum radius of an expanded artery to the radius of a normal artery, thanks to which the parameter examined can be described in a dimensionless way. Figure 17 presents the streamlines in the diastolic phase where the negative velocity gradient impacting the highest probability of boundary layer separation.

A similar analysis was made for the other groups. All the results have been included in Table 1. It is noticeable that for lower velocities, the use of a narrower

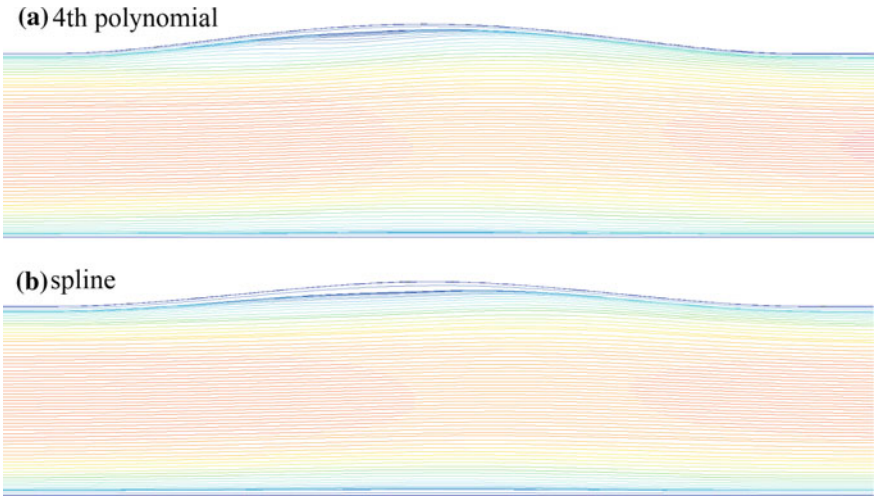

Fig. 15 Comparison of geometries: **a** fourth-degree polynomial **b** third-degree polynomial spline

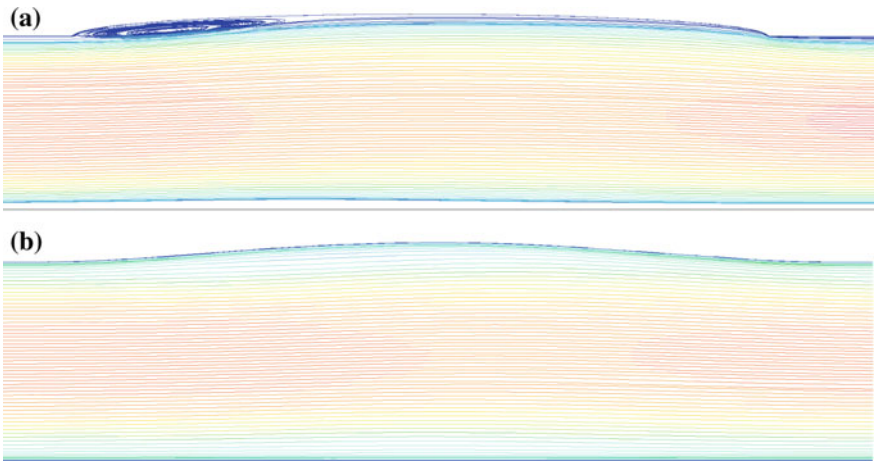

Fig. 16 Comparison of the artery geometry with the patch sewn in in the shape of **a** ellipse **b** polynomial

patch is required. This is due to the fact that slower blood flow enhances the growth of the viscosity forces. The higher viscosity forces in the fluid, the higher the tensions coagulating the fluid layers, which causes higher inclination of the fluid to separations and whirlpools. The final results assumed in the studies comprised the patch widths of lower velocity values, because they constitute a higher safety limit. The blood flow velocity, most of all, depends on the patient's pulse, artery diameter, and the difference in the value of the systolic and diastolic blood pressure. This value is variable, therefore the worst-case scenario method was applied (Fig. 18).

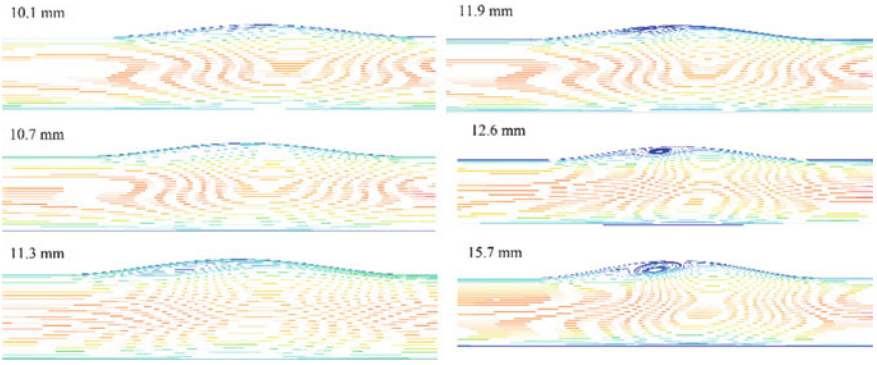

Fig. 17 The course of streamlines depending on the width of the patch [mm]

Table 1 Numerical results

Artery diameter (mm)	Velocity (m/s)	4th polynomial	3rd polynomial spine	Ellipse
8	0.4	10.6	10.6	12
	1	10.1	9.6	
10	0.4	12.6	11.3	
	1	11.3	10.1	
12	0.4	14.3	13.6	
	1	12.8	12.1	

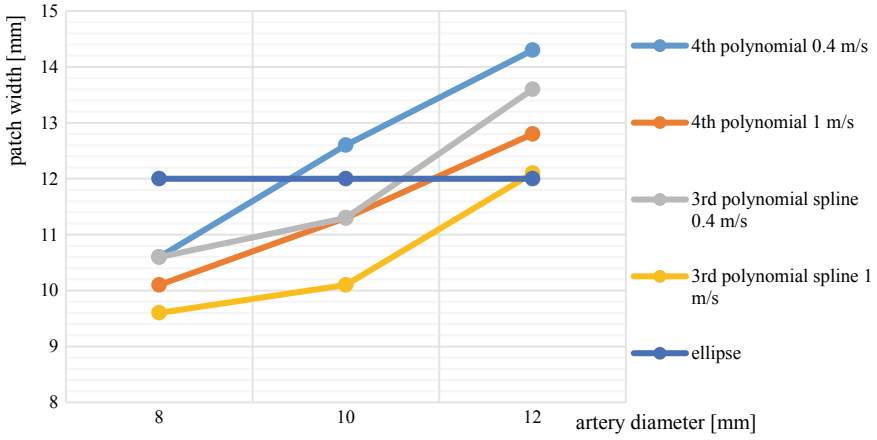

Fig. 18 Limit width of the patch depending on the diameter of the artery (velocity 0.4 m/s; 1 m/s)

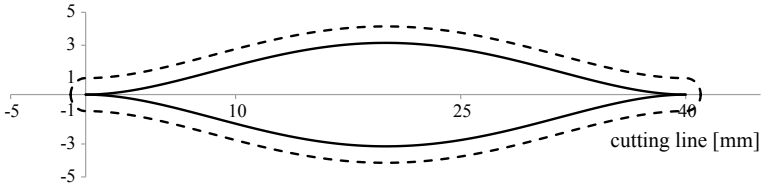

Fig. 19 Patch outline with overlap on the stitching (external profile) and without overlap on the stitching (internal profile), for the cutting length l = 40 mm, the width of the overlap on the suture s = 1 mm

The obtained values represent the starting points with a view to continuing and expanding the research. The final result will be the development of a complete patch geometry (Fig. 19), the insertion of which in the patient's artery would minimize the risk of plaque redeposition. The finished patch will be increased by 1 mm regarding the suturing technique. It will be customized to each individual patient. The studies carried out enabled the authors to determine the first input parameter: the patient's artery diameter. Finally, there will be more input parameters and they will consider the following: blood composition, carotid artery bifurcation angle, diameters of adjacent arteries (usually the main CCA and external ECA).

4 Conclusions

The performed analysis has shown that the most favorable geometry in terms of the flow is the artery expanded according to a polynomial function. Thanks to the appropriate formation of the walls, the lumen expands so gradually that the boundary layer increases slowly. While increasing the patch width, the risk of larger separations and reverse flow occurs. The larger the diameter of the patient's artery, in which the patch will be inserted, the larger the width that can be used (not exceeding 15 mm). Theoretically, the smaller the patch the better, since the artery geometry is not significantly changed. If, however, the patch sutured in is too small as a result of the patch shrinking, it may lead to a reduction of the arterial lumen. It is a more negative phenomenon than the expansion, because it restricts the blood flow. If plaque redeposition occurs in such an artery, it could be closed much sooner than with an expanded artery. Therefore, the information related to the width of the patch that can be applied is very important to the surgeons. The research allowed the authors to obtain widths that are justified analytically and mechanically.

The patches inserted thus far were similar to an ellipse or were of an irregular shape. They met their purpose, however, significantly affected the blood flow, which in some cases led to the necessity of subsequent surgery. The patches suggested in this paper have two basic advantages. The first is that the geometry of the patches has been described analytically, which enables their easy recovery with the use of simple aids. The other, more important aspect is the standardization of the geometry

of the inserted patches. The patches can be divided into several types adapted to the majority of patients and to the most commonly occurring diameters. Thanks to such a solution, the patches can be mass-produced in several variants. During the medical procedure, the surgeon would select a finished, ready-cut patch, depending on the patient's geometry. Hence, there would be no need to cut the patches while operating, which would reduce the time of the procedure and, most importantly, minimize the risk of restenosis.

References

1. May AG, Van de Berg L, Deweese JA, Rob CG (1963) Critical arterial stenosis. Surgery 54(1):250–259
2. Smoore W, Malone JM (1979) Effect of flow rate and vessel calibre on critical arterial stenosis1. J Surg Res 26 (1979)
3. Berguer R, Hwang NHC (1974) Critical Arterial Stenosis: A Theoretical and Experimental Solution. Ann Surg 180(1):39
4. Liapis CD, Bell SPRF, Mikhailidis D, Sivenius J, Nicolaides A, Fernandes e Fernandes J, Biasi G, Norgren L (2009) ESVS guidelines. invasive treatment for carotid stenosis: indications, techniques. Eur J Vasc Endovasc Surg
5. Muto A, Nishibe T, Dardik H, Dardik A (2009) Patches for carotid artery endarterectomy: current materials and prospects. J Vasc Surg 50(1):206–213
6. Rerkasem K, Rothwell PM (2009) Patch angioplasty versus primary closure for carotid endarterectomy. Cochrane Database Syst Rev
7. Chung TJ (2009) Computational fluid dynamics
8. Schäfer M (2006) Computational engineering: introduction to numerical methods
9. ANSYS: Ansys Fluent 14.0 tutorial guide (2009) Ansys INC
10. Botar CC, Vasile T, Sfrangeu S, Clichici S, Agachi PS, Badea R, Mircea P, Cristea MV (2010) Validation of CFD simulation results in case of portal vein blood flow. Comput Aided Chem Eng
11. Moyle KR, Antiga L, Steinman DA (2006) Inlet conditions for image-based CFD models of the carotid bifurcation: is it reasonable to assume fully developed flow? J Biomech Eng 128:371
12. Moon JY, Suh DC, Lee YS, Kim YW, Lee JS (2014) Considerations of blood properties, outlet boundary conditions and energy loss approaches in computational fluid dynamics modeling. Neurointervention
13. Steinman DA, Robarts JP, Milner JS, Moore JA, Rutt BK (1997) Hemodynamics of human carotid artery bifurcations: computational studies with models reconstructed from magnetic resonance imaging of normal subjects
14. Chien S, Usami S, Dellenback RJ, Gregersen MI (1967) Blood viscosity: influence of erythrocyte deformation. Science (80) 157:827–829
15. Chen J, Lu X-Y, Wang W (2006) Non-Newtonian effects of blood flow on hemodynamics in distal vascular graft anastomoses. J. Biomech. 39
16. Khan MF, Quadri ZA, Bhat SP (2013) Study of Newtonian and non-Newtonian effect of blood flow in portal vein in normal and hypertension conditions using CFD technique. Int J Eng Res Technol 6:974–3154
17. Boyd J, Buick JM, Green S (2007) Analysis of the Casson and Carreau-Yasuda non-Newtonian blood models in steady and oscillatory flows using the lattice Boltzmann method. Phys Fluids
18. Siebert MW, Fodor PS (2009) Newtonian and Non-Newtonian blood flow over a backward-facing step—a case study. In: Proceedings of the COMSOL Conference 2009, Boston